STAR Protocols

CellPress
OPEN ACCESS

Protocol

Protocol for isolating mice skeletal muscle myoblasts and myotubes via differential antibody validation

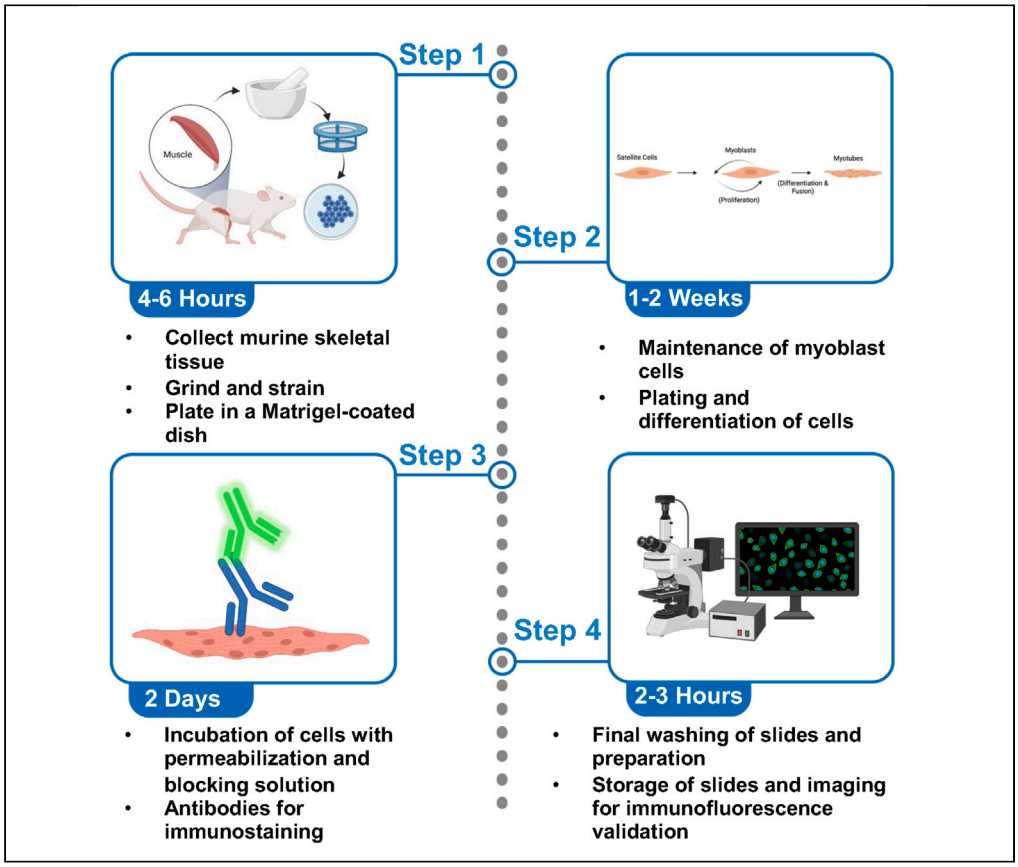

Isolation of skeletal muscles allows for the exploration of many complex diseases. Here, we present a protocol for isolating mice skeletal muscle myoblasts and myotubes that have been differentiated through antibody validation. We describe steps for collecting and preparing murine skeletal tissue, myoblast cell maintenance, plating, and cell differentiation. We then detail procedures for cell incubation, immunostaining, slide preparation and storage, and imaging for immunofluorescence validation.

Publisher's note: Undertaking any experimental protocol requires adherence to local institutional guidelines for laboratory safety and ethics.

Dominique C. Stephens, Margaret Mungai, Amber Crabtree, ..., Jamaine Davis, Steven M. Damo, Antentor O. Hinton, Jr.

sdamo@fisk.edu (S.M.D.)
antentor.o.hinton.jr@vanderbilt.edu (A.O.H.)

Highlights

Reproducible protocol for isolation of skeletal muscle myoblasts and myotubes

Isolate satellite cells to use for techniques such as electron microscopy

Confirmation of isolation through light microscopy techniques

Examine differences between myoblasts and myotubes

Stephens et al., STAR Protocols 4, 102591 December 15, 2023
https://doi.org/10.1016/j.xpro.2023.102591

STAR Protocols

CellPress
OPEN ACCESS

Protocol

Protocol for isolating mice skeletal muscle myoblasts and myotubes via differential antibody validation

Dominique C. Stephens,[1,2,11] Margaret Mungai,[3,11] Amber Crabtree,[1,11] Heather K. Beasley,[1] Edgar Garza-Lopez,[3] Larry Vang,[1] Kit Neikirk,[1] Zer Vue,[1] Neng Vue,[1] Andrea G. Marshall,[1] Kyrin Turner,[2] Jian-qiang Shao,[4] Bishnu Sarker,[5] Sandra Murray,[6] Jennifer A. Gaddy,[7,8] Jamaine Davis,[9] Steven M. Damo,[2,10,*] and Antentor O. Hinton, Jr.[1,10,12,13,*]

[1]Department of Molecular Physiology and Biophysics, Vanderbilt University, Nashville, TN 37232, USA

[2]Department of Life and Physical Sciences, Fisk University, Nashville, TN 37232, USA

[3]Department of Internal Medicine, University of Iowa, Iowa City, IA 52242, USA

[4]Central Microscopy Research Facility, University of Iowa, Iowa City, IA 52242, USA

[5]School of Applied Computational Sciences, Meharry Medical College, Nashville, TN 37232, USA

[6]Department of Cell Biology, College of Medicine, University of Pittsburgh, Pittsburgh, TN 15260, USA

[7]Division of Infectious Diseases, Vanderbilt University School of Medicine, Nashville, TN, USA

[8]Tennessee Valley Healthcare Systems, U.S. Department of Veterans Affairs, Nashville, TN, USA

[9]Department of Biochemistry and Cancer Biology. Meharry Medical College, Nashville, TN, USA

[10]Senior author

[11]These authors contributed equally

[12]Technical contact

[13]Lead contact

*Correspondence: sdamo@fisk.edu (S.M.D.), antentor.o.hinton.jr@vanderbilt.edu (A.O.H.)
https://doi.org/10.1016/j.xpro.2023.102591

SUMMARY

Isolation of skeletal muscles allows for the exploration of many complex diseases. Here, we present a protocol for isolating mice skeletal muscle myoblasts and myotubes that have been differentiated through antibody validation. We describe steps for collecting and preparing murine skeletal tissue, myoblast cell maintenance, plating, and cell differentiation. We then detail procedures for cell incubation, immunostaining, slide preparation and storage, and imaging for immunofluorescence validation.

BEFORE YOU BEGIN

Skeletal muscles (SkM) allow for animals and humans to be mobile,[1] serving many important roles and constituting nearly half of the total mass of the adult human body.[2] Defects in skeletal muscle mass can cause atrophy and other pathological diseases.[3] Beyond only mediating glucose uptake in an insulin-dependent manner, skeletal muscle also plays important roles in the metabolism and development of diabetes.[4] Since the first description of skeletal muscle diseases,[5] there have been numerous discoveries describing their pathology and the next step in studying these pathologies is characterizing the different cellular populations residing within them. Isolating cells from these muscles allows for models to develop more complex studies to understand how these pathological mechanisms work. In addition to muscle diseases, skeletal muscles are also used to study immunological, neuronal, and other chronic diseases.[6] While past studies have used immortalized myogenic cells, myoblasts offer unique advantages to understanding the process of myogenesis, which is an avenue for the repair of injured myofibers.[7] Specifically, skeletal muscle cells are essential for studies on exercise and insulin stimulation. They are also useful experimental models to answer more complex questions, such as the effects of insulin stimulation[8] on organelle morphology and the

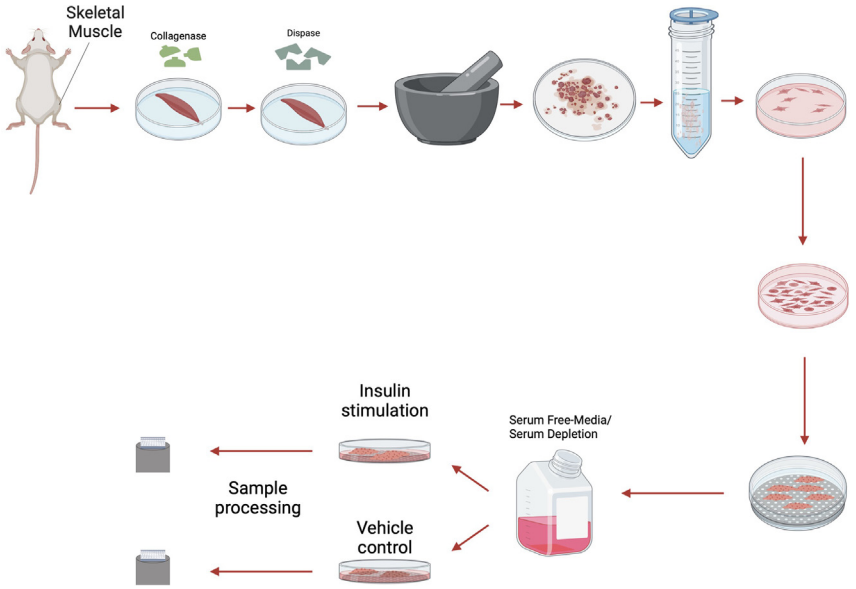

Figure 1. The process of myoblast isolation from gastrocnemius muscle

efficacy of new microscopy methods like Focused Ion Beam Scanning Electron Microscopy (FIB-SEM).[9] Yet, protocols that allow for the differentiation and isolation of myotubes and myoblasts remain limited.

Here we offer two aims, firstly to show how to develop isolate myoblasts, or differentiated myotubes, from murine skeletal muscle (Figure 1). Secondly, developing antibody-based approaches for validating SkM cells has been a challenge. Here we also offer a technique for myoblast validation. Antibodies are useful for validating different populations of skeletal muscle cells. Antibodies allow researchers to study the diversity of muscle fibers and cells while providing important insights into cellular processes and disease development. Here, we listed common antibodies used to study different cell populations in SkM tissue (Table 1).

SkM tissue is composed of various cell types with different functions, including myoblasts and fibroblasts.[3] Skeletal myoblasts drive muscle regeneration after injury, while fibroblasts create extracellular matrix components and secrete growth factors[10] (Figure 2). Morphologically, fibroblasts are larger than myoblasts and contain more vesicles.[11] Beyond this, while mononuclear cells replicate, as they form sheets of multinucleated myotubes, proliferation is impaired and myogenin is elevated.[12] Myoblasts' process of differentiation mimics that of *in vivo* myogenesis, with the structure of myoblasts affecting that of differentiated myotubes.[13] Given that these populations have morphological differences,[14] validating the myoblast or myotube stage is of critical importance, especially for experiments that seek to study homogenous populations and fine ultrastructural changes. Here, we also present how antibodies and fluorescence light microscopy can be used to validate different cell populations in skeletal muscle tissue. However, before you begin care should be taken in experimental design and selection for which populations you want to obtain. Here, we propose a standardized approach to isolate and identify different skeletal muscle cell populations. Using these methods, we looked at the effects on insulin stimulation on oxygen consumption rate (OCR) and have verified past studies which have implicated changes in respiration following insulin stimulation in a potential optic atrophy protein-1 (OPA-1) mediated manner.[15]

Institutional permissions

Timing: Dependent on murine age study

Table 1. A list of antibodies and their respective antigens for skeletal muscle validation after isolation

Antibody Name	Antigen	IF/IHC Rec		Isotype	Antigen Species	Host Species	Positive Tested Species Reactivity	Info
BF-F3-s	Myosin heavy chain Type IIB	2-5 µg/mL	Monoclonal	MIgM	Bovine	mouse	Bovine, Mouse, Porcine, Rat, Sheep	
SC-71-s	Myosin heavy chain Type IIA	2-5 µg/mL	Monoclonal	MIgG1	Bovine	mouse	Bovine, Canine, Goat, Horse, Human, Mole, Mouse, Porcine, Rabbit, Rat, elephant seal, guinea pig, llama and goat muscle. Sheep	This antibody recognizes the fast twitch isoform MyHC IIA specifically in horses and rodents.
BA-D5-s	Myosin heavy chain Type I	2-5 µg/mL	Monoclonal	MIgG2b	Bovine	mouse	Bovine, Canine, Fish, Goat, Guinea Pig, Horse, Human, Lamb, Llama, Mouse, Porcine, Rabbit, Rat, Zebrafish	Muscle contraction
F5D-s	Myogenin	2-5 µg/mL	Monoclonal	MIgG1, kappa light chain	Rat	mouse	canine, Feline, Human, Mammal, Mouse, Porcine, Rat	This antibody immunoprecipitates deletion mutants containing a.a. 138–158, region immediately carboxy-terminal to the bHLH domain.
PAX7-s	Pax7	2-5 µg/mL	Monoclonal	MIgG1, kappa light chain	Chicken	mouse	Amphibian, Avian, Bovine, Canine, Fish, Goat, Human, Mouse, Ovine, Porcine, Quail, Rat, Turtle, Xenopus, Zebrafish	nuclei in adult skeletal muscle satellite cells
D3-s	Desmin, intermediate filament	2-5 µg/mL	Monoclonal	MIgA, kappa light chain	Chicken	mouse	Chicken, Hamster, Mouse, Rat	D3 also stained primary cultures of embryonic cardiac myocytes
9.1 ITGA7-s	Integrin alpha-7, extracellular domain	2-5 µg/mL	Monoclonal	MIgG2c	Human	mouse	Human	Alpha 7/beta-1 integrin is the primary laminin-1 receptor. This receptor is expressed in skeletal and cardiac muscle and certain tumor cells. The 9.1 antibody recognizes the extracellular domain of alpha 7 integrin in both native and denatured conformations.
JLT12-s	troponin T, fast skeletal muscle specific	2-5 µg/mL	Monoclonal	MIgG1	Rabbit	mouse	Axolotl, Bovine, Broad species, Chicken, Human, Rabbit, Rat	Paraformaldehyde fixation for immunostaining is recommended. JLT12 recognizes all Troponin T, fast skeletal muscle isoforms and doesn't recognize slow isoforms. This antibody was initially characterized in Lin et al. [Lin, J.J.-C., Feramisco, J.R., Blose, S.H., and Matsumura, F. (1984). Monoclonal antibodies to cytoskeletal proteins. In Monoclonal Antibodies and Hybridomas: Progress and Applications. (eds. R.H. Kennett, T.J. McKearn, and K.B. Bechtol) pp. 119–151, Plenum Press, New York].
MANEX46B (7G1)-s	dystrophin	2–5 µg/mL	Monoclonal	MIgG1	human	mouse	Human, Mouse	Stains muscle membranes (no staining of Duchenne muscle membrane) Frozen, unfixed sections. May not work on formalin-fixed tissue. Dilution: 1/4

The Table was obtained from https://dshb.biology.uiowa.edu/.

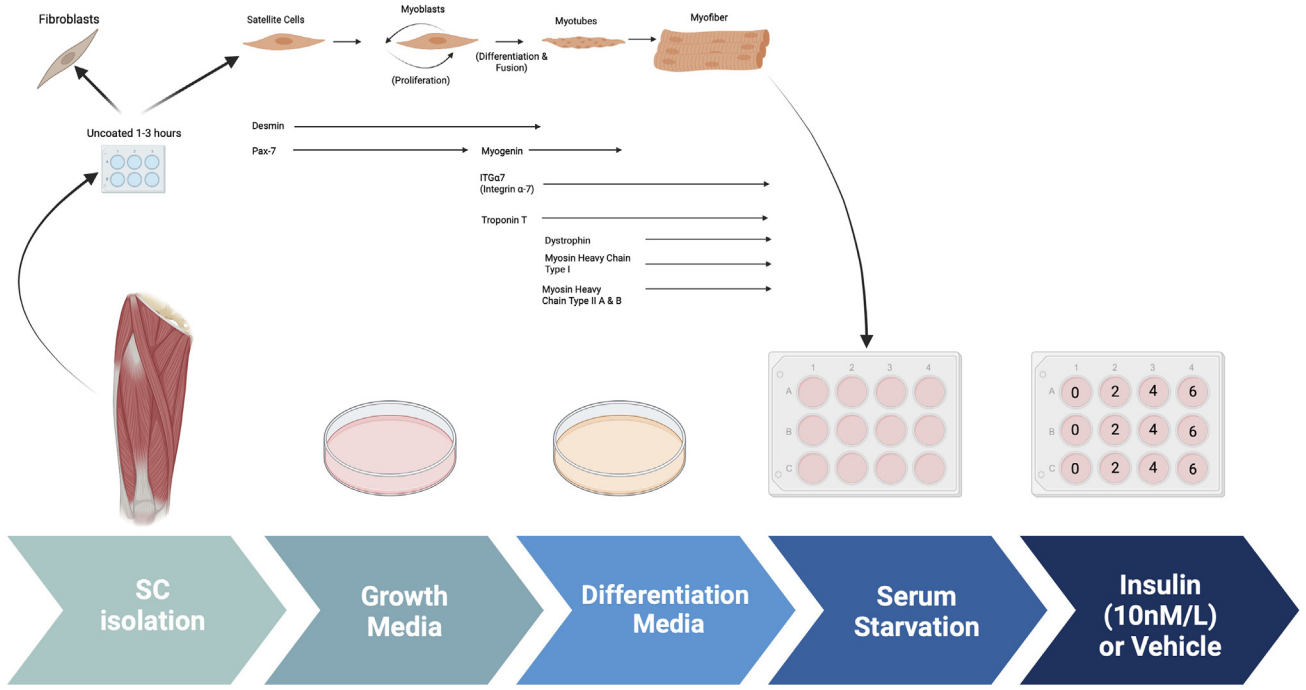

Figure 2. The process of myotube differentiation from myoblasts and utilization for serum

All mice utilized had a C57Bl/6J background. Mice studies followed previous studies by Pereira et al., Neikirk et al., and Lam et al.[16–18] with weaning at 3 weeks of age and maintained on standard chow (2920X Harlan Teklad, Indianapolis, IN, USA), and at 22°C with a 12 h light, 12 h dark cycle with free access to water and standard chow. All mouse experiments were conducted in alignment with the animal research guidelines from NIH and were approved by the University of Iowa IACUC.

KEY RESOURCES TABLE

REAGENT or RESOURCE	SOURCE	IDENTIFIER
Chemicals, peptides, and recombinant proteins		
4% paraformaldehyde	Thermo Fisher Scientific	J61899-AK
Beta-mercaptoethanol	Gibco	21985-023
Collagenase II	Gibco	17101015
DMEM (+ 4.5 g/L D-glucose, + L-Glut, – sodium pyruvate)	Gibco	11965-092
F-12 (+ L-Glut)	Gibco	11765-054
FBS	Atlanta Biologicals	S11550
Fungizone	Gibco	15290-018
Human FGF-basic (FGF-2/bFGF) recombinant protein	Thermo Fisher Scientific	13256-029
Insulin-transferrin-selenium-X (100×)	Gibco	41400045
MEM non-essential amino acids	Gibco	11140
PBS, pH 7.4	Gibco	10010023
Penicillin-Streptomycin	Gibco	15140
StemPro Accutase	Thermo Fisher Scientific	A1110501
Triton X-100 (1%)	Gibco	HFH10
Software and algorithms		
GraphPad	GraphPad Software, San Diego, California, USA	www.graphpad.com
ImageJ	Schindelin et al.[19]	https://imagej.net/
Experimental models: Organisms/strains		
Mouse: C57BL/6J WT (male and/or female mouse aged 8 weeks)	University of Iowa Animal Care Center	N/A

MATERIALS AND EQUIPMENT

Timing: 1 h

Prior to the protocol, make the following reagents and solutions and sterilize all equipment in an autoclave.

Initial PBS Wash mixture:

Make within 1 week prior to protocol, and store at 4°C until usage.

Name	Final concentration	Volume
PBS	N/A	25 mL
Fungizone	N/A	75 µL
Penicillin-Streptomycin	N/A	250 µL
Total:	N/A	25.325 mL

Initial DMEM-F12 incubation mixture:

Make within 1 week prior to protocol, and store at 4°C until usage.

Name		Volume
DMEM-F12	N/A	250 mL DMEM (+ 4.5 g/L D-glucose, + L-Glut, - Sodium Pyruvate) + 250 mL F-12 (+L-Glut)
Collagenase II	N/A	1300 mg
Penicillin-Streptomycin	N/A	6.4 mL
Fungizone	N/A	2.0 mL
Total:	N/A	508.4 mL

Secondary DMEM-F12 incubation mixture:

Make within 1 week prior to protocol, and store at 4°C until usage.

Name	Final concentration	Volume
DMEM-F12	N/A	250 mL DMEM (+ 4.5 g/L D-glucose, + L-Glut, - Sodium Pyruvate) + 250 mL F-12 (+L-Glut)
Collagenase II	N/A	650 mg
Penicillin-Streptomycin	N/A	6.4 mL
Fungizone	N/A	2.0 mL
Dispase	N/A	325 mg
Total:	N/A	508.4 mL

DMEM-F12 Growth Media:

Mix the following. Use a sterile filter with Millipore brand 0.22 µM filter units. Store at 4°C for no longer than 2 months. Add bFGF (10 ng/mL) to the aliquot just before adding it to plate.

Name	Final concentration	Volume
DMEM-F12	N/A	250 mL DMEM (+ 4.5 g/L D-glucose, + L-Glut, - Sodium Pyruvate) + 250 mL F-12 (+L-Glut)
FBS Note: Do not heat inactivate FBS. Just thaw, swirl to mix, and go.	N/A	129 mL
Penicillin-Streptomycin	N/A	6.4 mL

(*Continued on next page*)

Continued

Name	Final concentration	Volume
Fungizone	N/A	2.0 mL
MEM Non-essential Amino Acids	N/A	6.4 mL
Beta-Mercaptoethanol	N/A	6.4 μL
Total:	N/A	649.2 mL

Permeabilization Buffer:

Make within 1 week prior to protocol, and store at 4°C until usage.

Name	Final concentration	Volume
PBS	N/A	495.5 mL
Triton X-100	0.1%	0.5 mL
Total:	N/A	500 mL

Differentiation medium:

Make within 1 week prior to protocol, and store at 4°C until usage.

Name	Final concentration	Volume
DMEM (+ 4.5 g/L D-glucose, + L-Glut, - Sodium Pyruvate)	N/A	250 mL
F-12 (+L-Glut)	N/A	250 mL
FBS Note: Do not heat inactivate FBS. Just thaw, swirl to mix, and go.	N/A	10.5 mL
Insulin-transferrin-selenium-X (100×)	0.1%	5.3 mL
Total:	N/A	515.8 mL

Reconstitute Human FGF-basic (FGF-2/bFGF) Recombinant Protein (here we use Thermo Fisher Scientific 13256-029). Briefly, to prepare a stock solution of bFGF at a concentration of 0.1 mg/mL, reconstitute it in 100 μL of 10 mM Tris (pH 7.6). Dilute in buffer containing 0.1% BSA and store in polypropylene vials for up to six months at -20°C. Make aliquots to avoid repeated freezing and rethawing.

STEP-BY-STEP METHOD DETAILS

Myoblast isolation: Removal of muscle

Timing: 30 min

The below offers a basic text for the isolation of myoblast.

1. Following IACUC guidelines, euthanize mice.
2. Collect muscle tissue from the gastrocnemius, quadriceps, soleus, and hamstring muscles in both legs at 4–8 weeks of age from 4–6 mice.

   Note: Less or more mice can be utilized but we generally found batches of 4–6 to be a good quantity.

   ⚠ CRITICAL: This protocol works to make tissue-type specific cell lines. If the muscle types will not be combined, double the number of mice, to 8–12 mice, to ensure an adequate sample count.

3. Transfer the collected tissue to an Eppendorf tube.

Note: From this point on, ensure a sterile environment is utilized.

Myoblast isolation: Preparation of muscle, shaking, and grinding of tissue

Timing: 2.5 h

4. Wash isolated tissue 2–3 times with the initial PBS wash mixture.

Note: The PBS solution is prepared right before dissecting the tissue.

5. Incubate muscle tissue in the initial DMEM-F12 incubation mixture.

⚠ CRITICAL: Avoid filtering the DMEM-F12 media containing collagenase, 1% pen/strep, and 3 μL/mL Fungizone. This initial DMEM-F12 incubation mixture must be chilled (4°C) when added to reduce temperature shock.

6. Maintain the muscle solution in a 37°C water bath for 10–15 min.
7. Shake at 220 rpm, for an overall time of 1.5 h.
8. After incubation, wash the tissue 3–4 times with PBS.
9. Incubate in warmed secondary DMEM-F12 incubation mixture while the tissue is shaken for 30 min in a 37°C water bath.

Note: Secondary DMEM-F12 incubation mixture has to be pre-warmed to 37°C to ensure efficient mixing of dispase and since the muscles were at 37°C after incubation.

10. After shaking, grind tissue with a mortar and pestle in the presence of liquid nitrogen.
11. Pass through a 100 μm, then 70 μm, cell strainer.
12. Centrifuge the solution at 1000 rpm/27 rcf for 5 min to pellet the cells. Avoid doing longer for this step (see Problem #1)

Myoblast isolation: Plating

Timing: 1–3 h

The protocol below offers details to isolate myoblasts through plates.

13. Transfer the to a plate and resuspended using DMEM-F12 growth media supplemented with 40 ng/mL bFGF.
14. Pre-plate the cells for 1–3 h on UNCOATED dishes to reduce the number of fibroblasts.

⚠ CRITICAL: Fibroblasts can dilute satellite cells. Recommended for dystrophic or injured muscle. Pre-plating on an uncoated plate causes fibroblasts to stick and be isolated (see Problem #2). Fibroblasts can separately be used to isolate and for other experiments.

15. Dilute cells 1:15 in PBS, then plate in a Matrigel-coated dish.

Note: To create Matrigel-coated dishes, dilute stock concentration (while keeping on ice) to 1:15 in sterile PBS in the hood. Put Matrigel solution on flask/plate, shake/tilt to coat the bottom, incubate at 22°C (room temperature) in a chemical hood for 30 min, and remove Matrigel solution back into its original tube. Matrigel solution may be reused up to 5 times in total.

Myoblast isolation: Differentiation

Timing: 1–2 weeks

The below protocol offers subsequent differentiation to myotubes, if desired.

16. Wait for activation, which takes 24–48 h, after which myoblasts will grow rapidly.
    a. To maintain healthy myoblast cells, use the growth media supplemented with bFGF (10 ng/mL).

⚠ CRITICAL: Use Differentiation Medium to go from myoblasts to myocytes and then to myotubes (Figure 2).

17. Plate primary myoblast at ~.8 × 10^6 cells per well and to differentiate the cells, add differentiation media, supplemented with 1:10,000 bFGF.

Note: This will depend on # of cell passages and type of treatment, adjust accordingly.

18. Incubate for 4–7 days for differentiation to myotubes.

Note: Switch out with fresh differentiation media every 2 days, supplemented with 1:10,000 bFGF.

19. Cells are split using 2–5 mL of accutase for 5–15 min, dependent on cell count.
20. Optional: 3 days after differentiation, infect myotubes with GFP-expressing adenovirus per previous procedures,[16] if imaged with light microscopy.

Note: DO NOT use trypsin to split the cells. Accutase is less harsh to the extracellular matrix, surface proteins, and cytoskeleton of skeletal cells than trypsin, so it is highly preferred.[20] Accutate total incubation time and volume will differ depending on cell yield (see Problem #3).

21. Cells are maintained in (5% CO_2) at 37°C. If growing myotubes, a confluency of 70%–85% has to be reached prior to adding growth media.

Validation day 1: Permeabilization and blocking

Timing: 1.5 h

Immunofluorescence staining is effective for examining differences in skeletal muscles simultaneously. Refer to Table 1 for a list of validated primary antibodies for skeletal muscles. Select secondary antibodies that are compatible with the epifluorescence or confocal microscope available to you.

⚠ CRITICAL: All steps are performed at 22°C (room temperature) unless otherwise indicated.

Note: This protocol for Immunofluorescence staining and antibody validation of isolated skeletal muscle cells is an adaptation of Esper et al., skeletal muscle tissue immunofluorescence labeling protocol.[21]

22. Fix cells by incubating them in 4% paraformaldehyde (PFA) for 5 min.
23. Wash three times for 5 min using phosphate-buffered saline (PBS).

Note: Ice-cold 100% methanol or acetone is an effective fixative for cryosections and more suited for some antigens. Acetone is less harsh than methanol.

24. Incubate cells in permeabilization buffer for 10 min.
25. Incubate cells in blocking solution for 1 h at 22°C (room temperature) or up to 18 h overnight at 4°C.

Note: When using permeabilization buffer, keep the solution away from the hydrophobic barrier to avoid loss of hydrophobicity. If this happens, wash the slide well with PBS. Include Mouse on Mouse (MOM) blocking reagent at a 1:40 dilution when staining mouse tissue with antibodies raised in the mouse.

Validation day 2: Antibodies

Timing: 30 min

26. To begin immunostaining, dilute the primary and secondary antibodies in a blocking solution according to the manufacturer's suggested ratio.

Note: It is acceptable to dilute antibodies in hybridoma supernatant when targeting multiple antigens.

27. Aspirate the blocking buffer and cover the slide with the primary antibody solution.
28. Incubate the slides for up to 18 h (overnight) at 4°C.

Validation day 3: Preparing slides for imaging

Timing: 2–3 h

This final day prepares slides for imaging prior to final imaging, although imaging may be performed on this same day.

29. On the following day, wash three times for 5 min with PBS.
30. After washing, cover cells with secondary antibodies diluted in blocking buffer for 1 h at 22°C (room temperature) in the dark.

Note: Keep slides in the dark for the remainder of the protocol.

31. After incubation, wash the slides three times for 5 min with PBS.
32. Incubate the cells with 1 μg/mL DAPI diluted in PBS for 5 min.
33. Wash once with PBS for 5 min.
34. Aspirate the PBS and place 1–2 drops of mounting media onto the cells
35. Carefully place a coverslip on the slide, while avoiding air bubbles.
36. Let the slides dry in the dark for 1–2 h before sealing the slides with clear nail polish.
37. Store the slides at 4°C and image within 2 weeks.

Light microscopy studies

Timing: 2–6 h

All imaging experiments were performed at Central Microscopy Research Facility, University of Iowa, while adenoviruses were obtained from University of Iowa Viral Vector Core facility.

38. Plate myotubes on 35 mm dishes with a glass bottom and imaged for light microscopy.
39. Perform staining of myotubes on Olympus IX-81 (done in this protocol) or equivalent.

Seahorse analyzer studies

Timing: 2–3 days

This is a well-reported procedure that may be found in more depth per established protocols.[16,22] Oxygen consumption rate was measured for using an XF24 bioanalyzer (Seahorse Bioscience: North Billerica, MA, USA), as previously described.[16,22]

40. Plate Myotubes and myoblasts at a density of 20 × 10^3 per well and differentiate for 3 days (in step by step above).
41. Treat isolated myotubes and myoblasts with 10 nmol/L insulin for the specified time.[15]
42. Replace media with XF-DMEM (supplemented with 1 g/L D-Glucose, 0.11 g/L sodium pyruvate, and 4 mM L-Glutamine) and deprive cells of CO_2 for 60 min.
43. Perform oligomycin (1 μg/mL), carbonyl cyanide 4-(trifluoromethoxy)phenylhydrazone (FCCP; 1 μM), rotenone (1 μM), and antimycin A (10 μM) treatment. For quantifications, time points 1–3 measure basal respiration, or baseline rate of oxygen consumption by cells in culture without any treatment. Add Oligomycin (1 μg/mL) to inhibit ATP synthase, which reduces mitochondrial respiration and leads to an increase in proton gradient, to measure the amount of oxygen consumed by the myoblasts and myotubes to maintain the proton gradient in time points 4–6. Add carbonyl cyanide 4-(trifluoromethoxy)phenylhydrazone (FCCP; 1 μM) in time points 7–9, which allows electrons to flow freely through the electron transport chain allowing for measurements of reserve capacity and maximum oxygen consumption. Finally, add rotenone (1 μM) and antimycin A (10 μM) in time points 10–12, which inhibit electron transfer from NADH to ubiquinone and ubiquinol to cytochrome c, respectively, to measure non-mitochondrial respiration.[23]
44. For normalization of proteins, after measurement, add 20 μL of 10 mM Tris with 0.1% Triton X-100 at pH 7.4 to lyse cells per prior protocols,[22] and replace with 480 μL of Bradford reagent.

Transmission electron microscopy

Timing: 2–3 days

This is a well-reported procedure that may be found in more depth per established protocols.[17,24]

45. Once Myoblasts and myotubes are isolated according to the step-by-step above, place them in six-well poly-D-lysine-coated plates for TEM processing per established protocols.[17,24].
46. Fix cells by incubating at 37°C with 2.5% glutaraldehyde in 0.1 m sodium cacodylate buffer for 1 h.
47. Rinse twice with 0.1 m sodium cacodylate buffer, prior to fixation at 22°C (room temperature) for 30 min to 1 h using 1% osmium tetroxide and 1.5% potassium ferrocyanide in 0.1 m sodium cacodylate buffer.
48. Wash samples for 5 min with 0.1 m sodium cacodylate buffer (7.3 pH), then diH_2O (2 × 5 min).
49. Incubate samples with 2.5% uranyl acetate, diluted with H_2O, at 4°C for up to 18 h (overnight).
50. Dehydrate samples and replace ethanol with Eponate 12 mixed in 100% ethanol in a 1:1 solution for 30 min at RT. Repeat three times for 1 h using 100% Eponate 12, replace media, and cure in an oven at 70°C for up to 18 h (overnight).
51. After cracking and submerging the plate in liquid nitrogen, use an 80 nm thickness jeweler's saw to cut the block to fit in a Leica UC6 ultramicrotome sample holder.
52. From there, place sections section on formvar-coated copper grids.
53. Counterstain grids in 2% uranyl acetate for 2 min and Reynold's lead citrate for 2 min.

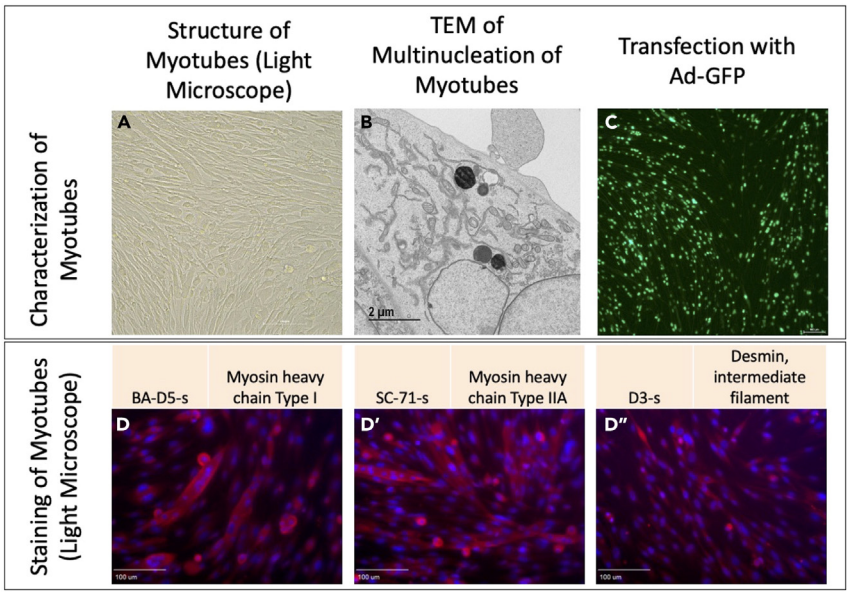

Figure 3. Validation of myotube differentiation via light microscopy

(A–C) Myotubes as characterized by (A) Light microscopy, (B) Transmission electron microscopy, and (C) Transfection with adenovirus containing the green fluorescent protein gene (Ad-GFP).

(D) Straining with BA-D5-s, D′ SC-71-s, and D″ D3-s to show myosin and desmin.

54. Acquire by TEM on either a JEOL JEM-1230, operating at 120 kV, or a JEOL 1400, operating at 80 kV (used for these representative data), our equivalent.
55. Perform analysis and quantification via protocols by Lam et al. (2021).[18]

EXPECTED OUTCOMES

Upon isolation of myoblast and differentiation into myotubes, we validated their structure in light microscopy (Figure 3A). Furthermore, we viewed multinucleated myotubes through TEM to validate the ultrastructure (Figure 3B). Transfection further showed myotubes demonstrated fluorescence as expected (Figure 3C). From there, we performed staining for myosin and desmin, muscle-specific proteins that play crucial roles in muscle cell structure and function,[25] to confirm that filaments were present (Figure 3D-D″).

Once myoblasts and myotubes are validated, they can be used for a variety of studies including to measure mitochondrial efficiency with oxygen consumption rate, western blot analysis to look for expression of specific proteins in knockout studies, or a variety of electron microscopy techniques such as serial block-face scanning electron microscopy to perform 3D reconstruction of organelles (Figure 4). In the past, following this isolation and differentiation protocol, we have successfully used the protocol by Garza-Lopez et al. (2022)[26] for 3D reconstruction and quantification of mitochondria and endoplasmic reticulum, alongside the protocol by Neikirk et al. (2023)[17] for 3D reconstruction and quantification of lipid droplets, lysosomes, and autophagosomes. However, from our experience, any validated scanning electron microscopy protocol should be effective following isolation and differentiation.

As an example, to validate this method, we sought to understand how insulin treatment (10 nM/L) in 2-h increments may alter myoblast and myotube function through the usage of a Seahorse XF96 analyzer, per past protocols.[27] We found that for myoblasts, there is a significantly increased basal, maximum, and non-mitochondrial OCR after 2 h of insulin treatment, while this difference is retained or exacerbated after 4 h of insulin treatment (Figures 5A and 5B). After 6 h of insulin treatment, OCR conversely showed significant decreases in all of these parameters (Figure 5C). In myotubes, after 2

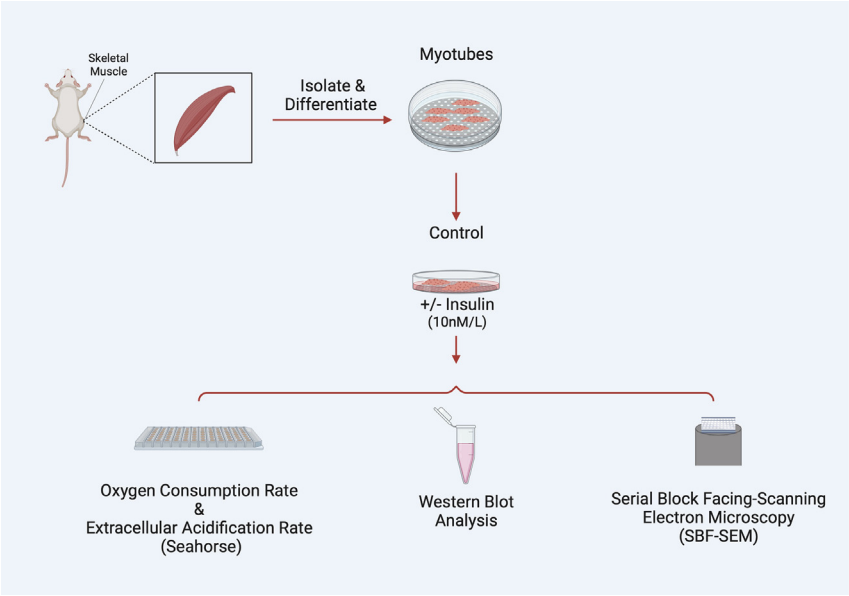

Figure 4. Examples of experiments that may be performed following myotube differentiation and isolation

and 4 h of insulin treatment, we similarly noted a significant increase in mitochondrial OCR (Figures 5D and 5E). Notably, the increase in basal, ATP-linked, maximum, and non-mitochondrial OCR is much higher in 4 h than 2 h. Unlike myoblasts, 6 h of insulin treatment myotubes did not differ significantly from untreated cells (Figure 5F). Importantly, there may be a differential response to insulin treatment in myoblasts and myotubes, highlighting the importance of studying both models. This validated that the function of myoblasts and myotubes are intact following this isolation.

From there we sought to elucidate if organelle proteins are affected following insulin treatment and we targeted Optic atrophy protein 1 (OPA-1), which is a mitochondrial inner membrane (IMM) fusion protein that mediates the fusion of the IMM between two mitochondria while also serving roles in mitochondrial bioenergetics and cristae architecture.[28] OPA-1 is just one of several proteins which modulate mitochondrial structure. For example, contrastingly, Dynamin-related protein 1 (DRP-1) is a protein that initiates the fission process through constriction of the mitochondria which divides the mitochondria into two separate organelles.[29] However, given that OCR increased following insulin treatment, it is possible this is due to the increased mitochondrial area caused by upregulated mitochondrial fusion. To see if OPA-1 may be changed in expression, we performed western blotting. When looking at OPA-1, we noticed a significant continuous increase in protein levels in myoblasts across 2 and 4 h of insulin stimulation when normalized (Figures 6A and 6B). We further differentiated primary myotubes and carried out these experiments again to see if any differences existed (Figures 6C and 6D). We noticed significant increases in OPA-1 levels after 4 h of insulin stimulation (Figures 6C and 6D). Together, this suggests that insulin stimulation causes increased expression of OPA-1 in a short time frame which is exacerbated in myotubes compared with myoblasts.

Since we saw changes in OPA-1 expression, which is known to trigger fusion, we also validated this technique of myoblasts and myotubes isolation through the quantification of mitochondria and cristae[18] following insulin treatment. Using transmission electron microscopy, we compared mitochondrial morphology without (Figure 7A) and with 2-h insulin treatment in myoblasts (Figure 7A′). When quantified we saw that mitochondria reduce in number (Figure 7B), while becoming less spherical and larger in area (Figures 7C and 7D). Together, this suggests an uptick in fusion following insulin treatment in myoblasts. We also considered how cristae morphology may be affected following insulin treatment (Figures 7E and 7E′) and we saw that although the cristae score, a

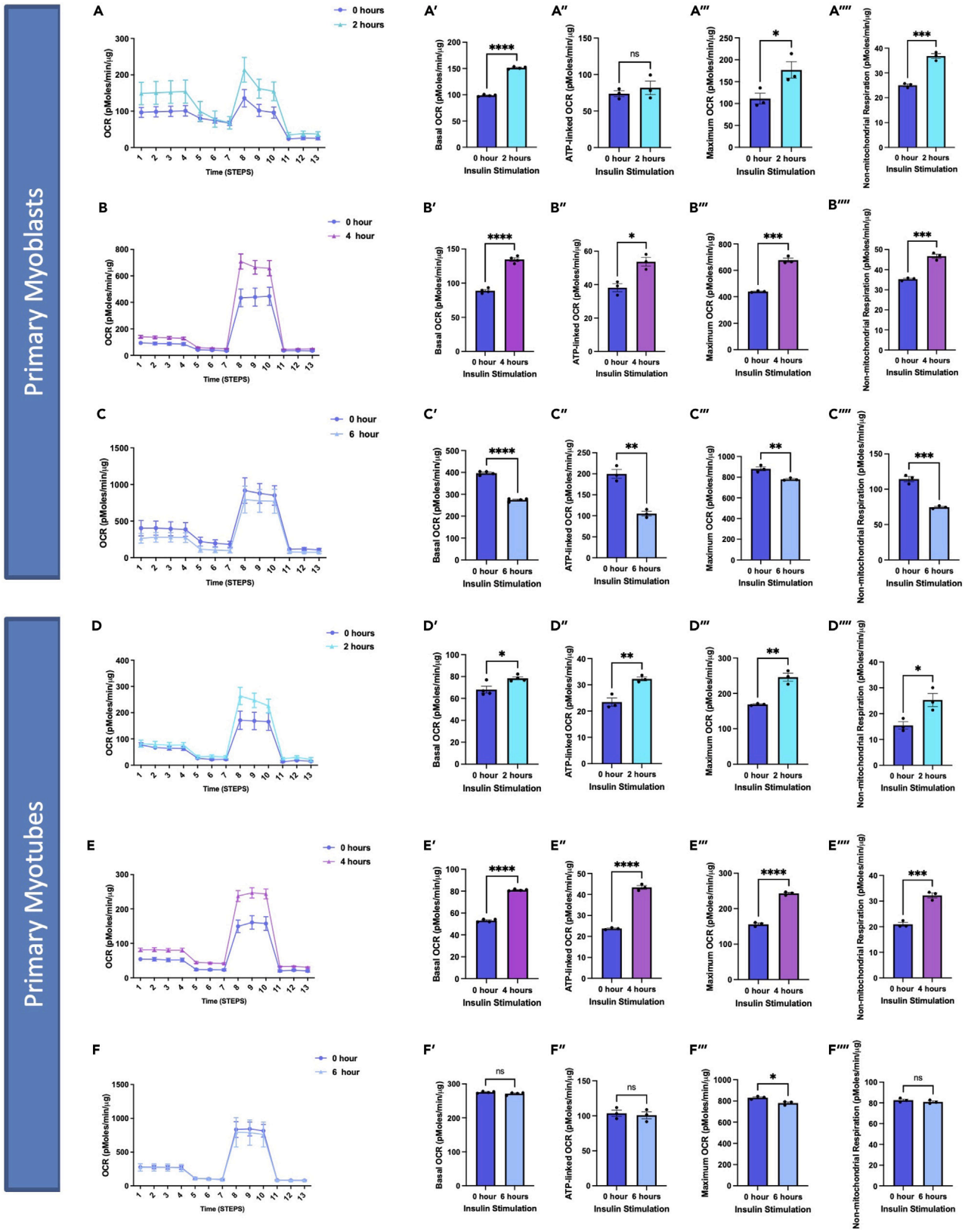
Primary Myoblasts
Primary Myotubes
A
0 hours
2 hours
OCR (pMoles/min/µg)
Time (STEPS)
A′
Basal OCR (pMoles/min/µg)
****
0 hour 2 hours
Insulin Stimulation
A″
ATP-linked OCR (pMoles/min/µg)
ns
A‴
Maximum OCR (pMoles/min/µg)
*
A⁗
Non-mitochondrial Respiration (pMoles/min/µg)
***
B
0 hour
4 hour
B′
B″
B‴
B⁗
C
0 hour
6 hour
C′
C″
**
C‴
C⁗
D
0 hours
2 hours
D′
D″
D‴
D⁗
E
0 hours
4 hours
E′
E″
E‴
E⁗
F
0 hour
6 hour
F′
F″
F‴
F⁗

Figure 5. Oxygen consumption rate (OCR) altered in myoblasts and myotubes upon altered insulin stimulation which shows changes in mitochondrial efficiency

(A–C) (A) Seahorse plot for primary myoblasts following 2 h of insulin stimulation (B) 4 h of insulin stimulation and (C) 6 h of insulin stimulation.
(D–F) (D) Oxygen consumption rate was measured after several inhibitors to measure respiration in primary myotubes after 2 h, (E) 4 h, and (F) 6 h of insulin stimulation. (A′-F′) Basal OCR, which represents respiration under normal, unstressed conditions. (A″-F″) ATP-linked OCR, which is respiration associated with ATP synthesis during oxidative phosphorylation, which is marked by a reduction in OCR due to oligomycin. (A‴-F‴) Maximum OCR, which is the maximal capacity at which mitochondria may utilize oxygen. (A⁗-F⁗) Non-mitochondrial respiration, which can be attributed to factors such as glycolysis or ROS and not due to mitochondrial respiration. These values were compared to the control (blue) in all of these examples. Data are represented as mean ± SEM. N = 6 per treatment, and * indicates p-value < .05.

measurement of relative cristae quality, did not change, cristae number and area increased suggesting a greater capacity for oxidative function (Figures 7F–7H). From there, we similarly sought to see if mitochondria in myotubes had changed following insulin stimulation (Figure 8A and 8A′). Similar to myoblasts, we saw while mitochondria decrease, their size increases (Figures 8B–8D), again indicating increased mitochondrial fusion. When evaluating the cristae structure, we noticed that while similar to myoblasts cristae score was unchanged, the cristae number had a more significant increase (Figures 8E–8G). Similar to myoblasts, the cristae area also increased following 2 h of insulin stimulation (Figure 8F). Together these quantifications show that changes in OCR may be due to OPA-1-mediated changes in mitochondrial and cristae architecture following insulin stimulation.

Together these data validate this isolation and validation technique allows for the application of experimental models to elucidate cellular processes. This demonstrates the viability of the protocol outlined here for skeletal muscle. After differentiation, quantification can be done for many experimental designs. Here, we performed seahorse analysis per prior methods[27] with GraphPad to perform students' T-tests to measure statistical significance.

Past results have demonstrated that myoblasts can be assayed through staining with Pax7 and MyoD, while multinucleated myotubes are visualized with phase contrast microscopy or after staining for myosin heavy chain.[7] Past protocols are also available which allow for incredibly dense populations of myoblasts (1.5×10^7, 200 times cell expansion) to be obtained through an intelligent culture system with suppression of myotube formation.[12] Another technique has also allowed for 1×10^7–2×10^7 myoblasts to be isolated from murine hindlimbs from a single organism without the need for cell straining or sorting.[30] Tangentially, techniques allow for induced pluripotent stem cells to be differentiated into myotubes which allow for the study of insulin resistance.[31] Our technique is advantageous in offering the ability to obtain either subpopulation, as well as fibroblasts, allowing for a wide range of experiments to perform. Further, the study of specific genes in myoblasts and myotubes can then be affected through verified techniques such as adenovirus, or herpes simplex virus type 1 amplicon vectors, depending on the specific gene.[32]

QUANTIFICATION AND STATISTICAL ANALYSIS

For all analyses, GraphPad Prism software package was used (La Jolla, CA, USA), with black bars representing the standard error of meanwhile dots represent individual data points shown. If only two groups were used for comparison, an unpaired t-test was the statistical test, while more than two groups were compared with a one-way ANOVA and Tukey *post hoc* tests for multiple comparisons, or their non-parametric equivalent if applicable. A minimum threshold of $p < 0.05$ indicated a significant difference.

LIMITATIONS

This protocol has been optimized for mice gastrocnemius, quadriceps, and hamstring muscles and may not be applicable to other model organisms or tissue types. Compared with other protocols, ours takes a similar period of time,[30] but this can still be a slow process that must be carried out across multiple days. While C2C12 myoblasts are ideal for this protocol, increasingly human skeletal myoblasts are important to study, and past protocols indicate that differences in the procedure must

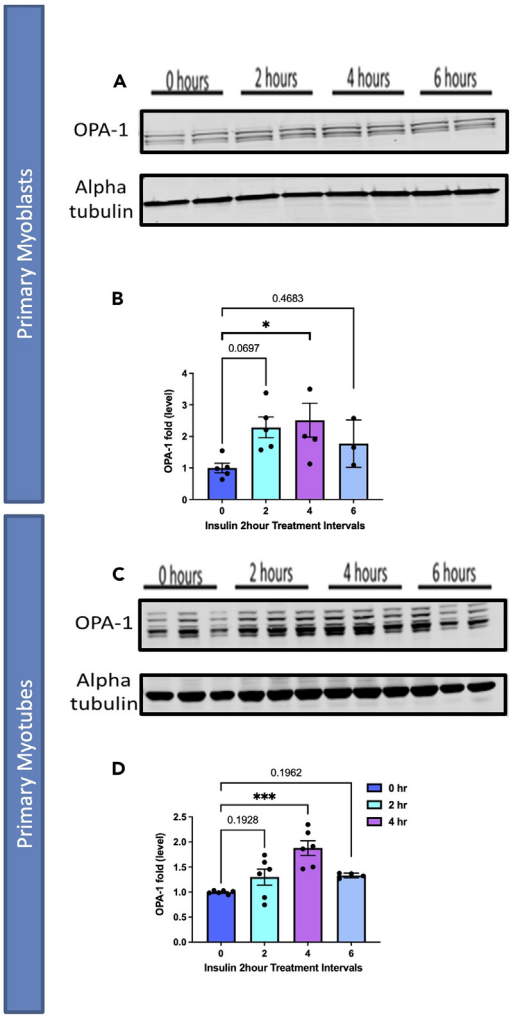

Figure 6. Comparison of mitochondrial fusion proteins following insulin stimulation in primary myoblasts and myotubes

(A) Western blotting for mitochondrial fusion protein OPA-1 following 2 h, 4 h, and 6 h of insulin stimulation.

(B) OPA-1 levels normalized to Alpha tubulin following insulin stimulation.

(C) This was replicated in primary myotubes, as western blotting for mitochondrial fusion OPA1.

(D) OPA-1 levels, normalized to Alpha tubulin, in primary myotubes following insulin treatment. Data are represented as mean ± SEM. N = 6 per treatment, and * indicates p-value < .05.

be made, such as antisense miR-133a addition, to promote the fast differentiation of human skeletal myoblasts.[33]

TROUBLESHOOTING

Problem 1

Ultrastructure or Gross morphology of Myoblasts is Degraded.

Potential solution

This may be due to too much damage incurred to myoblasts during preparation. We found that optimizing the process by first digesting tissue with type II collagenase and dispase, followed by grinding the tissue in liquid nitrogen with a mortar with a pestle, and passing it through cell strainers resulted in an improved procedure. However, reducing the time grounded or reducing the amount of digestion can avoid potential damage to the myoblasts if it is occurring.

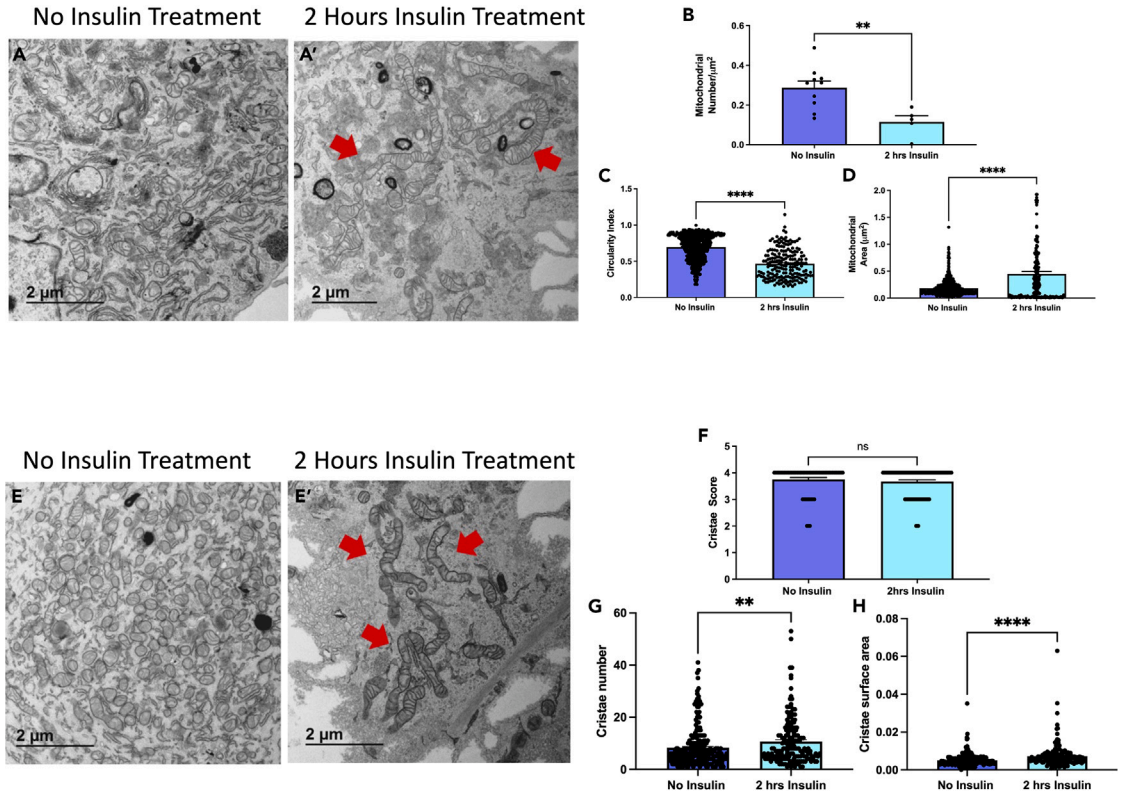

Figure 7. TEM quantification of myoblasts

(A) Representative transmission electron micrographs from control and (A′) insulin-treated cells, with red arrows showing fused mitochondria.

(B–D) (B) Quantifications of number of mitochondria, (C) circularity of mitochondria, (D) and area of mitochondria.

(E) Representative transmission electron micrographs from control and (E′) insulin-treated cells, with red arrows showing cristae.

(F–H) (F) Quantifications from cristae score, (G) cristae quantity, and (H) cristae area comparing non-insulin and insulin-treated myoblasts. Data are represented as mean ± SEM. Scale bars are 2 μm. Dots show the number of samples. ** and **** indicates $p < 0.01$ and $p < 0.0001$, respectively.

Problem 2

Contamination with Fibroblasts.

Potential solution

It is important to plate first on an uncoated plate. However, if fibroblasts are still observed, pre-plating can be done twice. Antibody-based selection of fibroblasts may cause certain issues but can also be explored as an option to remove fibroblasts. If this remains an issue, other methods have shown that using flowing cytometry can be used to identify and remove fibroblasts.[34]

Problem 3

Low Cell Yield or Viability.

Potential solution

If myoblast or myotube viability is low, it is important to increase the concentration of growth factors and ensure a sterile environment is maintained. Reducing time with accutase can also ensure cells are not treated too harshly.

RESOURCE AVAILABILITY

Lead contact

Further information and requests for resources and reagents should be directed to and will be fulfilled by the lead contact, Antentor Hinton (antentor.o.hinton.jr@Vanderbilt.Edu).

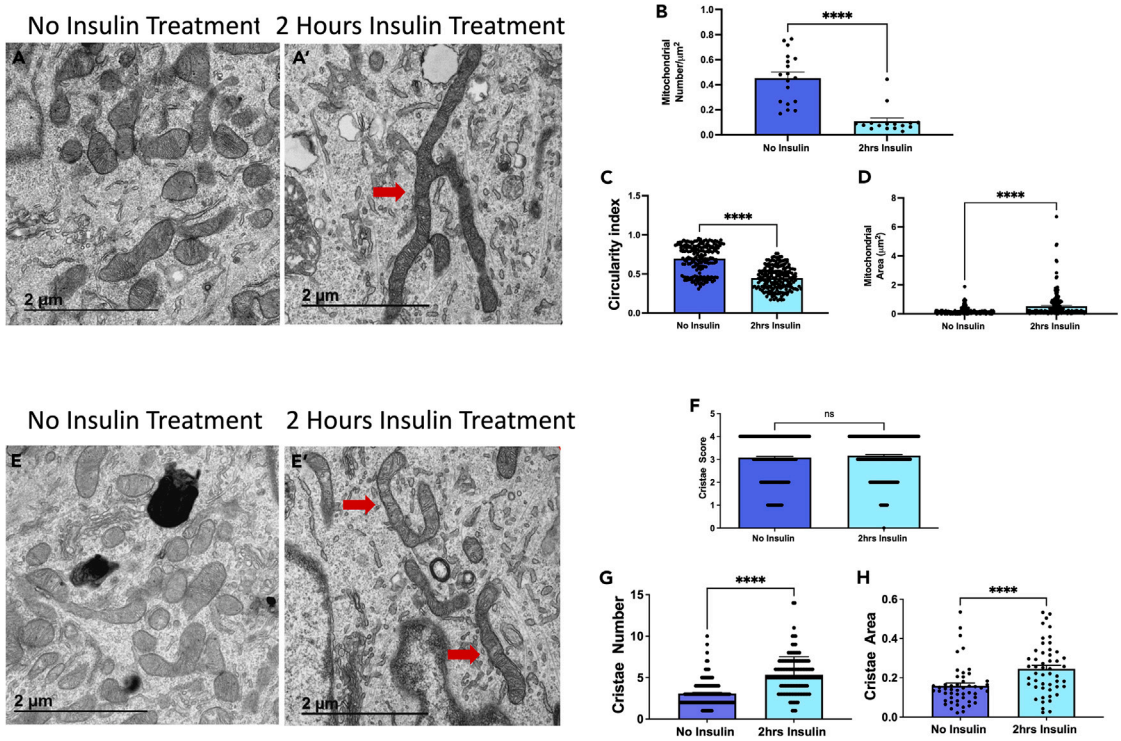

Figure 8. TEM quantification of myotubes

(A) Representative transmission electron micrographs from control and (A′) insulin-treated cells, with red arrows showing fused mitochondria.
(B–D) (B) Quantifications of number of mitochondria, (C) circularity of mitochondria, (D) and area of mitochondria.
(E) Representative transmission electron micrographs from control and (E′) insulin-treated cells, with red arrows showing cristae.
(F–H) (F) Quantifications from cristae score, (G) cristae quantity, and (H) cristae area comparing non-insulin and insulin-treated myotubes. Data are represented as mean ± SEM. Scale bars are 2 µm. Dots show the number of samples. ** and **** indicates $p < 0.01$ and $p < 0.0001$, respectively.

Materials availability

All generated materials, if applicable, are created in methods highlighted in the text above.

Data and code availability

Full data utilized and requests for data and code availability should be directed to and will be fulfilled by the lead contact, Antentor Hinton (antentor.o.hinton.jr@Vanderbilt.Edu).

ACKNOWLEDGMENTS

All antibodies were obtained from the Iowa Developmental Studies Hybridoma Bank (DSHB). This project was funded by the UNCF/Bristol-Myers Squibb E.E. Just Faculty Fund, BWF Career Awards at the Scientific Interface Award, BWF Ad-hoc Award, NIH Small Research Pilot Subaward 5R25HL106365-12 from the National Institutes of Health PRIDE Program, DK020593, and Vanderbilt Diabetes and Research Training Center for DRTC Alzheimer's Disease Pilot & Feasibility Program; CZI Science Diversity Leadership (grant number 2022-253529) from the Chan Zuckerberg Initiative DAF, an advised fund of Silicon Valley Community Foundation (to A.O.H.J.); NSF EES2112556, NSF EES1817282, and CZI Science Diversity Leadership (grant number 2022-253614) from the Chan Zuckerberg Initiative DAF, an advised fund of Silicon Valley Community Foundation (to S.M.D.); and National Institutes of Health (grant HD090061) and the Department of Veterans Affairs Office of Research award I01 BX005352 (to J.A.G.). Additional support was provided by the Vanderbilt Institute for Clinical and Translational Research Program, supported by the National Center for Research Resources (grant UL1 RR024975–01) and the National Center for Advancing Translational

Sciences (grant 2 UL1 TR000445–06), and the Cell Imaging Shared Resource. BioRender was used for the creation of figures.

AUTHOR CONTRIBUTIONS

D.C.S.: Experimental design, data collection, data analysis, and manuscript writing/editing. M.M.: Experimental design, data collection, data analysis, and manuscript writing/editing. A.C.: Experimental design, data collection, data analysis, and manuscript writing/editing. H.K.B.: Laboratory experiments and data collection.E.G.-L.: Microscopy and imaging expertise. L.V.: Experimental support and data analysis. K.N.: Laboratory experiments, manuscript writing, and manuscript editing. Z.V.: Experimental support and data analysis. N.V.: Experimental support and data editing. A.G.M.: Project coordination and manuscript editing.K.T.: Research assistance and data analysis. J.Q.S.: Microscopy and imaging expertise. B.S.: Computational analysis and modeling. SM: Manuscript writing. JAG: Manuscript writing. J.D.: Manuscript writing. S.M.D.: Project leadership and manuscript editing. A.O.H.J.: Principal investigator, project conception, and manuscript writing.

DECLARATION OF INTERESTS

The authors declare no competing interests.

REFERENCES

1. Figueiredo, P.A., Mota, M.P., Appell, H.J., and Duarte, J.A. (2008). The role of mitochondria in aging of skeletal muscle. Biogerontology *9*, 67–84. https://doi.org/10.1007/s10522-007-9121-7.

2. Ostrovidov, S., Hosseini, V., Ahadian, S., Fujie, T., Parthiban, S.P., Ramalingam, M., Bae, H., Kaji, H., and Khademhosseini, A. (2014). Skeletal Muscle Tissue Engineering: Methods to Form Skeletal Myotubes and Their Applications. Tissue Eng. Part B Rev. *20*, 403–436. https://doi.org/10.1089/ten.teb.2013.0534.

3. Dave, H.D., Shook, M., and Varacallo, M. (2022). Anatomy, Skeletal Muscle. In StatPearls [Internet] (StatPearls Publishing).

4. Vepkhvadze, T.F., Vorotnikov, A.V., and Popov, D.V. (2021). Electrical Stimulation of Cultured Myotubes in vitro as a Model of Skeletal Muscle Activity: Current State and Future Prospects. Biochemistry. *86*, 597–610. https://doi.org/10.1134/S0006297921050084.

5. Walusinski, O. (2022). François-Amilcar Aran (1817-1861) and the recognition of spinal muscular atrophy. Rev. Neurol. *178*, 756–765. https://doi.org/10.1016/j.neurol.2022.01.011.

6. Morgan, J., and Partridge, T. (2020). Skeletal muscle in health and disease. Dis. Model. Mech. *13*, dmm042192. https://doi.org/10.1242/dmm.042192.

7. Hindi, L., McMillan, J.D., Afroze, D., Hindi, S.M., and Kumar, A. (2017). Isolation, Culturing, and Differentiation of Primary Myoblasts from Skeletal Muscle of Adult Mice. Bio. Protoc. *7*, e2248. https://doi.org/10.21769/BioProtoc.2248.

8. Alonge, K.M., Meares, G.P., and Hillgartner, F.B. (2017). Glucagon and Insulin Cooperatively Stimulate Fibroblast Growth Factor 21 Gene Transcription by Increasing the Expression of Activating Transcription Factor 4. J. Biol. Chem. *292*, 5239–5252. https://doi.org/10.1074/jbc.M116.762922.

9. Marshall, A.G., Damo, S.M., and Hinton, A. (2023). Revisiting focused ion beam scanning electron microcopy. Trends Biochem. Sci. *48*, 585–586. https://doi.org/10.1016/j.tibs.2023.02.005.

10. Thummarati, P., and Kino-Oka, M. (2020). Effect of Co-culturing Fibroblasts in Human Skeletal Muscle Cell Sheet on Angiogenic Cytokine Balance and Angiogenesis. Front. Bioeng. Biotechnol. *8*, 578140. https://doi.org/10.3389/fbioe.2020.578140.

11. Yablonka-Reuveni, Z., Anderson, S.K., Bowen-Pope, D.F., and Nameroff, M. (1988). Biochemical and morphological differences between fibroblasts and myoblasts from embryonic chicken skeletal muscle. Cell Tissue Res. *252*, 339–348. https://doi.org/10.1007/BF00214376.

12. Kino-oka, M., Chowdhury, S.R., Muneyuki, Y., Manabe, M., Saito, A., Sawa, Y., and Taya, M. (2009). Automating the Expansion Process of Human Skeletal Muscle Myoblasts with Suppression of Myotube Formation. Tissue Eng. Part C Methods *15*, 717–728. https://doi.org/10.1089/ten.tec.2008.0429.

13. Berendse, M., Grounds, M.D., and Lloyd, C.M. (2003). Myoblast structure affects subsequent skeletal myotube morphology and sarcomere assembly. Exp. Cell Res. *291*, 435–450. https://doi.org/10.1016/j.yexcr.2003.07.004.

14. Mingueitti, G., and Mair, W.G. (1980). The developing human muscle: ultrastructural differences between myoblasts and fibroblasts. Rev. Bras. Pesqui. Med. Biol. *13*, 1–8.

15. Parra, V., Verdejo, H.E., Iglewski, M., del Campo, A., Troncoso, R., Jones, D., Zhu, Y., Kuzmicic, J., Pennanen, C., Lopez-Crisosto, C., et al. (2014). Insulin Stimulates Mitochondrial Fusion and Function in Cardiomyocytes via the Akt-mTOR-NFκB-Opa-1 Signaling Pathway. Diabetes *63*, 75–88. https://doi.org/10.2337/db13-0340.

16. Pereira, R.O., Tadinada, S.M., Zasadny, F.M., Oliveira, K.J., Pires, K.M.P., Olvera, A., Jeffers, J., Souvenir, R., Mcglauflin, R., Seei, A., et al. (2017). OPA 1 deficiency promotes secretion of FGF 21 from muscle that prevents obesity and insulin resistance. EMBO J. *36*, 2126–2145.

17. Neikirk, K., Vue, Z., Katti, P., Rodriguez, B.I., Omer, S., Shao, J., Christensen, T., Garza Lopez, E., Marshall, A., Palavicino-Maggio, C.B., et al. (2023). Systematic Transmission Electron Microscopy-Based Identification and 3D Reconstruction of Cellular Degradation Machinery. Adv. Biol.e2200221 https://doi.org/10.1002/adbi.202200221.

18. Lam, J., Katti, P., Biete, M., Mungai, M., AshShareef, S., Neikirk, K., Garza Lopez, E., Vue, Z., Christensen, T.A., Beasley, H.K., et al. (2021). A Universal Approach to Analyzing Transmission Electron Microscopy with ImageJ. Cells *10*, 2177. https://doi.org/10.3390/cells10092177.

19. Schindelin, J., Arganda-Carreras, I., Frise, E., Kaynig, V., Longair, M., Pietzsch, T., Preibisch, S., Rueden, C., Saalfeld, S., Schmid, B., et al. (2012). Fiji: an open-source platform for biological-image analysis. Nat. Methods *9*, 676–682.

20. Nowak-Terpiłowska, A., Śledziński, P., and Zeyland, J. (2021). Impact of cell harvesting methods on detection of cell surface proteins and apoptotic markers. Braz. J. Med. Biol. Res. *54*, e10197. https://doi.org/10.1590/1414-431X202010197.

21. Esper, M.E., Kodippili, K., and Rudnicki, M.A. (2023). Immunofluorescence Labeling of Skeletal Muscle in Development, Regeneration, and Disease. Methods Mol. Biol. *2566*, 113–132. https://doi.org/10.1007/978-1-0716-2675-7_9.

22. Dranka, B.P., Benavides, G.A., Diers, A.R., Giordano, S., Zelickson, B.R., Reily, C., Zou, L., Chatham, J.C., Hill, B.G., Zhang, J., et al. (2011). Assessing bioenergetic function in response to oxidative stress by metabolic profiling. Free

Radic. Biol. Med. *51*, 1621–1635. https://doi.org/10.1016/j.freeradbiomed.2011.08.005.

23. Rose, S., Frye, R.E., Slattery, J., Wynne, R., Tippett, M., Pavliv, O., Melnyk, S., and James, S.J. (2014). Oxidative Stress Induces Mitochondrial Dysfunction in a Subset of Autism Lymphoblastoid Cell Lines in a Well-Matched Case Control Cohort. PLoS One *9*, e85436. https://doi.org/10.1371/journal.pone.0085436.

24. Hinton, A., Katti, P., Christensen, T.A., Mungai, M., Shao, J., Zhang, L., Trushin, S., Alghanem, A., Jaspersen, A., Geroux, R.E., et al. (2023). A Comprehensive Approach to Sample Preparation for Electron Microscopy and the Assessment of Mitochondrial Morphology in Tissue and Cultured Cells. Adv. Biol.e2200202 https://doi.org/10.1002/adbi.202200202.

25. Agnetti, G., Herrmann, H., and Cohen, S. (2022). New roles for desmin in the maintenance of muscle homeostasis. FEBS J. *289*, 2755–2770. https://doi.org/10.1111/febs.15864.

26. Garza-Lopez, E., Vue, Z., Katti, P., Neikirk, K., Biete, M., Lam, J., Beasley, H.K., Marshall, A.G., Rodman, T.A., Christensen, T.A., et al. (2021). Protocols for Generating Surfaces and Measuring 3D Organelle Morphology Using Amira. Cells *11*, 65. https://doi.org/10.3390/cells11010065.

27. Pereira, R.O., Marti, A., Olvera, A.C., Tadinada, S.M., Bjorkman, S.H., Weatherford, E.T., Morgan, D.A., Westphal, M., Patel, P.H., Kirby, A.K., et al. (2021). OPA1 deletion in brown adipose tissue improves thermoregulation and systemic metabolism via FGF21. Elife *10*, e66519. https://doi.org/10.7554/eLife.66519.

28. Barrera, M., Koob, S., Dikov, D., Vogel, F., and Reichert, A.S. (2016). OPA1 functionally interacts with MIC60 but is dispensable for crista junction formation. FEBS Lett. *590*, 3309–3322. https://doi.org/10.1002/1873-3468.12384.

29. Peng, L., Men, X., Zhang, W., Wang, H., Xu, S., Xu, M., Xu, Y., Yang, W., and Lou, J. (2011). Dynamin-related protein 1 is implicated in endoplasmic reticulum stress-induced pancreatic β-cell apoptosis. Int. J. Mol. Med. *28*, 161–169. https://doi.org/10.3892/ijmm.2011.684.

30. Shahini, A., Vydiam, K., Choudhury, D., Rajabian, N., Nguyen, T., Lei, P., and Andreadis, S.T. (2018). Efficient and high yield isolation of myoblasts from skeletal muscle. Stem Cell Res. *30*, 122–129. https://doi.org/10.1016/j.scr.2018.05.017.

31. Iovino, S., Burkart, A.M., Warren, L., Patti, M.E., and Kahn, C.R. (2016). Myotubes derived from human-induced pluripotent stem cells mirror in vivo insulin resistance. Proc. Natl. Acad. Sci. USA *113*, 1889–1894. https://doi.org/10.1073/pnas.1525665113.

32. Wang, Y., Fraefel, C., Protasi, F., Moore, R.A., Fessenden, J.D., Pessah, I.N., DiFrancesco, A., Breakefield, X., and Allen, P.D. (2000). HSV-1 amplicon vectors are a highly efficient gene delivery system for skeletal muscle myoblasts and myotubes. Am. J. Physiol. Cell Physiol. *278*, C619–C626. https://doi.org/10.1152/ajpcell.2000.278.3.C619.

33. Cheng, C.S., El-Abd, Y., Bui, K., Hyun, Y.-E., Hughes, R.H., Kraus, W.E., and Truskey, G.A. (2014). Conditions that promote primary human skeletal myoblast culture and muscle differentiation in vitro. Am. J. Physiol. Cell Physiol. *306*, C385–C395. https://doi.org/10.1152/ajpcell.00179.2013.

34. Stellato, M., Czepiel, M., Distler, O., Błyszczuk, P., and Kania, G. (2019). Identification and Isolation of Cardiac Fibroblasts From the Adult Mouse Heart Using Two-Color Flow Cytometry. Front. Cardiovasc. Med. *6*, 105.